TRABAJO DE FIN DE GRADO:

Statistical analysis of microlensing light curves

Ana Esteban Gutiérrez

Tutorized by : Evencio Mediavilla Gradolph

September, 2016

• University of La Laguna. Science Faculty, Physics Section •

- Department of Astrophysics -

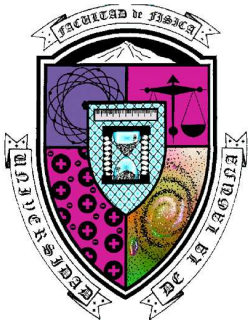

Abstract

En este proyecto de fin de Grado, exploraremos el uso del efecto *lente gravitatoria en quásares* como una herramienta para estudiar las velocidades peculiares de las galaxias que actúan como lente.

Este trabajo está dividido en dos partes: en primer lugar, trataremos el estudio de la magnificación inducida por el efecto lente en los movimientos relativos de las imágenes múltiples de un quasar; en segundo lugar, realizaremos simulaciones del número de picos generados por el efecto microlente en las curvas de luz de las imágenes de un quásar.

En la primera parte, usaremos una serie de códigos desarrollados en el lenguaje Python para simular los movimientos relativos de las imágenes resultantes de los sistemas quásar con efecto lente, cuantificando los desplazamientos entre las imágenes y discutiendo su posible detección.

Por otro lado, los principales objetivos de la segunda parte son la simulación de las curvas de luz de las imágenes de un quasar a partir de sus mapas de magnificación inducida por el efecto microlente y el recuento de los máximos relativos que aparecen en las curvas de luz. La frecuencia de estos máximos estará relacionada con la velocidad peculiar de la galaxia.

Finalmente, dos resultados interesantes de este trabajo son las expectativas de desplazamiento de decenas de $\mu as/año$ en casos favorables (lentes de alta magnificación) y que el error en la medida del número de cuentas de máximos relativos en curvas de luz, es similar o ligeramente inferior al error Poissoniano.

Contents

1 Introduction

Gravitational Lenses (GL) are very useful tools in Astrophysics and Cosmology nowadays. They are an essential part of the theoretical and experimental basis of the General Theory of Relativity. In the context of the present work, they are also interesting because of the mathematical and computational properties related to their study. The scientific community uses Gravitational Lenses as invaluable tools for drawing and studying the mass distribution in different scales in a Universe where the majority of the matter has an unknown nature. In addition, it is known that GL also magnify space (and, hence, fluxes) acting as a natural optical magnifying system.

Even though the term of Gravitational Lens is the most used one by astronomers to describe this kind of phenomenon, the expression of Gravitational Mirage approaches better to its own nature. The atmospheric mirages occur when there is a modification in the direction of the light, caused by a variation in the refractive index. If we attend to the Fermat's principle, it says that the light tends to look for the faster way of moving between two points. Nevertheless, the faster way in the atmosphere don't use to be a straight line. As the velocity is higher in the cold air, the light will follow a curved trajectory searching the coldest layers in the atmosphere. In certain circumstances, when the temperature changes strongly and the object and the observer are very far away, then the light is able to find more than one way to connect the object and the observer. In that case, we could see more than one image from a distant object which is a result of this spectacular phenomenon of the curvature of the light rays.

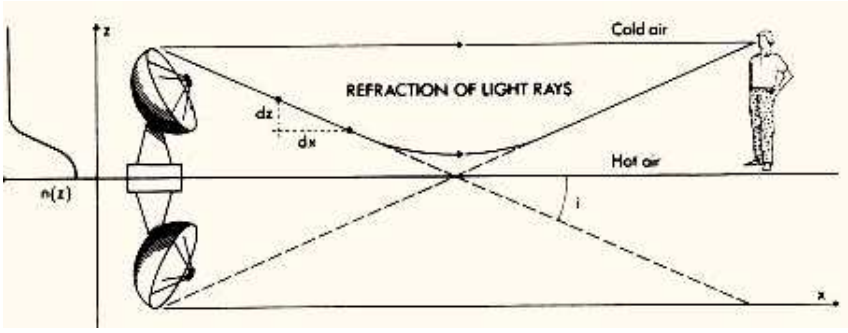

Gravity can also deflect light rays. In a Gravitational Mirage, the gravity is the responsible of bending the light rays. In fact, one of the most outstanding results of the General Theory of Relativity is the deflection of the light rays. This effect and the dilation of time in presence of a gravitational field are two of the essential predictions of the General Theory of Relativity, which set the basic phenomenology of the GL. However, long before the developing of this theory, it was suspected that gravity influences the behavior of light.

In order to delve into the history of the GL, we must take a look to the past and in particular, to the early 1704, when Newton had already supposed the existence of a bending of the starlight due to the gravitational field coming from a massive object when the light rays pass

near it. This idea was included in the Corpuscular Theory of Light, specifically in his book 'Optiks'. All the same, Einstein was the first scientist who calculated the correct value for light bending in his General Theory of Relativity in the 20th century. However, Einstein expressed the low probability of discovering two stars enough aligned as to generate a lens system. In 1919, Eddington and Dyson went to an expedition to take advantage of a solar eclipse in order to measure the displacement of the apparent positions of the stars induced by the gravitational field of the Sun. The results achieved there, made Einstein and his theory of general relativity world-famous. Furthermore, gravitational lensing is discussed by Eddington in his book "Space, Time, and Gravitation", which was published in 1920. In 1937, Fritz Zwicky proposed galaxies as better lenses than stars, because they are more likely to be gravitationally lensed. That is, the necessary near-alignment of a distant object (a source), a closer object (a lens) and an observer on Earth is much more probable for galaxies than for stars.

In 1964 Sjur Refsdal proposes to use Gravitational Lenses for measuring masses and calculating Hubble's constant. Also, he and Kyongae Chang predicted the microlensing effect by stars in the gravitational lens in 1979 and took the first step for the study of quasar microlensing. In the same year and 60 years after the famous Eddington expedition, the astronomers discovered a double image from a distant quasar called Q0957+561, caused by the gravitational field of an intervening galaxy which acts as a gravitational lens. This first identification of a gravitational lens was soon followed by others: in 1985 a cuadruple system called QSO 2237+0305 was discovered. It became one of the most famous gravitational lenses and its popular name is Einstein's cross. These discoveries were sucessfully achieved because bright and remote quasars are ideal sources to be imaged by an intervening lens galaxy. Today, more than 100 lensed quasars are known.

It is customary to consider three different types of lens effect: Strong Lens Effect, Weak Lens Effect and Microlensing Effect. In this work we want to focus on quasar microlensing, which is a combination of Strong Lensing and Microlensing. On the one hand, we are interested in the images of a quasar separated a few arcsecs by the large mass ($10^{10}\,M_{\odot}$) of the intervening galaxy (when the source and the lens are well aligned we would not see a discrete group of images, but a continuous ring or a broken ring composed by a few arcs).

On the other hand, we are also interested in the effect in each of these images of the granulation of the lens galaxy mass distribution in stars (about $1\,M_{\odot}$). This microlensing effect will not generate observable multiple images, but it can change the brightness of each one of the images of the lensed quasar.

1.1 The lens equation

In this section we are going to present the basic mathematical description of the phenomenon of gravitational lensing.

In the scheme below we have represented: the distant source (S), the object which creates the gravitational field (i.e., the lens, L), and the observer (O). The plane that contains the lens is the lens plane and the other plane which contains the source is the source plane. If our object (a galaxy, for instance) does not generate a gravitational field, the light would follow a straight line from S to O (dashed line). This trajectory would form an angle β with the optical axis (OL). However, in presence of the galaxy's gravitational field (L), the light rays will feel an atraction to the galaxy and then, they will not follow a straight line anymore. Instead of it, they will be bent approaching to L. This trajectory can be approximated by two straight lines (SM and MO). The observer will see that the light comes from the direction MO with an angle θ wth respect to OL and he will give a position S1 to the source. The angle α is the deflection angle between SM (initial trayectory) and MO (final trajectory).

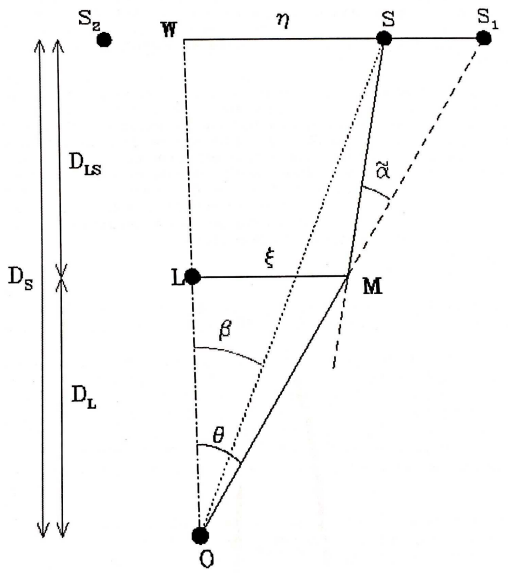

In the source plane we will have,

$$\eta = WS_1 - SS_1 \tag{1.1}$$

and taking into account that there is a similarity in the triangles,

$$\frac{WS_1}{D_S} = \frac{\xi}{D_L} \tag{1.2}$$

and considering that the deflection angle is very small, from the triangle MSS_1 we can write:

$$\alpha = \frac{SS_1}{D_{LS}}, \tag{1.3}$$

therefore, if we substitude (1.2) and (1.3) in the equation (1.1), we have:

$$\eta = \frac{D_S}{D_L}\xi - D_{LS}\alpha \tag{1.4}$$

We can rewrite this expression using: $\eta = \beta D_S$, $\xi = \theta D_L$,

$$\theta D_S = \beta D_S + \alpha D_{LS} \tag{1.5}$$

The lens equation can also be written in a vectorial form as:

$$\overrightarrow{y} = \overrightarrow{x} - \overrightarrow{\alpha}(\overrightarrow{x}) \tag{1.6}$$

where

$$\overrightarrow{y} \equiv \frac{\overrightarrow{\eta}}{\eta_0}, \overrightarrow{x} \equiv \frac{\overrightarrow{\xi}}{\xi_0}$$

and $\eta_0 \equiv \xi_0 \frac{D_S}{D_L}$. ξ_0 is a characteristic distance scale in the lens plane which is chosen according to the type of lens, in order to obtain an adimensional equation.

1.2 Magnification

It is important to introduce now the magnification effect of lensing. Lensing can magnify and distort the image of the background source. We define magnification as the parameter which indicates how much the flux of an object increases due to the lens effect. The flux depends on the product of the intensity and the solid angle, $\Delta F = I\Delta\Omega$, and according to Liouville's theorem, the lens effect does not affect to the intensity. Thus all the magnification is related to the solid angle, $\Delta\Omega \propto \Delta S/R^2$. Consequently, the magnification arises from the variation

of the differential element of area induced by the gravitational lens effect. We can write the magnification as:

$$\mu = \frac{dx^1 dx^2}{dy^1 dy^2} \tag{1.7}$$

if we consider the transformation between surface diferentials, we will get:

$$dy^1 dy^2 = dx^1 dx^2 \left| \frac{\partial y^i}{\partial x^j} \right| \tag{1.8}$$

where $\left|\partial y^i / \partial x^j\right|$is the Jacobian determinant of the transformation.

Then, the magnification will be:

$$\mu = \left| \frac{\partial y^i}{\partial x^j} \right|^{-1} \equiv \left| A^{ij} \right|^{-1} \tag{1.9}$$

It is very common to write the matrix A in terms of two parameters: the convergence, κ , and the shear, γ. According to the lens equation, the matrix A can be defined as:

$$A^{ij} = \frac{\partial y^i}{\partial x^j} = \delta^i_j - \frac{\partial \alpha^i}{\partial x^j} = \begin{pmatrix} 1-\kappa-\gamma_1 & \gamma_2 \\ \gamma_2 & 1-\kappa+\gamma_1 \end{pmatrix} \tag{1.10}$$

The points where $|A| = 0$ have, theoretically, infinite magnification. There will be a singularity there and the transformation $\overrightarrow{y} = \overrightarrow{y}(\overrightarrow{x})$ will not be invertible (its Jacobian determinant vanishes). In the lens plane we will have one dimensional regions called critical curves whose transformed in the source plane are the regions called caustic curves. Then, sources on a caustic region, will have a magnification formally infinite. Thus, when a pointlike source crosses a caustic, we will observe a very sharp event of high magnification. However, if the source is extended, we will see a peak which can be rather smooth when the source is large.

2 Gravitational lensing simulations

The first step in our study of GL is to write a computer code in order to simulate a gravitational lens system. The generation of the images for a given source and lens pair will be our first goal. The code was written using the Python programming language and the algorithm is based on the inverse ray shooting method (IRS method).

2.1 Images

If we want to determine the position of the images ($\overrightarrow{x}$) from the position of the source ($\overrightarrow{y}$) we would have to solve equation (1.6), in general trascendent and multi-valued. The deflection angle, $\overrightarrow{\alpha}(\overrightarrow{x})$, given in the adimensional equation (1.6) depends on the kind of lens and it can be very complicated (in this work we are going to consider the point like lens to represent stars and the singular isothermal sphere plus an external perturbation lens, SIS+γ, to represent galaxies). However, using eq. (1.6) we can inmediately obtain a point in the source plane, $\overrightarrow{y}$, given a point in the image plane, $\overrightarrow{x}$. In what follows, we will make use of this inversion.

To start with the code of the program, we assign the coordinates of the source and the lens, respectively, to the vectors: $\overrightarrow{y} = (y_1, y_2)$; $\overrightarrow{x} = (x_1, x_2)$. As commented above, depending on the explicit relationship between the deflection angle α and $\overrightarrow{x}$, $\overrightarrow{\alpha}(\overrightarrow{x})$, and also on the source position, $\overrightarrow{y}$, the lens equation would have one or many solutions: $\overrightarrow{x}\,(\overrightarrow{y})$ (images). In general, this equation is not analitically invertible and the procedure to obtain the solutions or images, $\overrightarrow{x}\,(\overrightarrow{y})$, can be a difficult problem of numerical calculation. However, we can simulate the gravitational lens effect by using the inverse ray shooting method. In first place, we set the pixels matrix which defines the image : $I(x_1, x_2)$. The lens equation allows us to obtain univocally the coordinates of each point (x_1, x_2) in the source plane, $(y_1(x_1, x_2), y_2(x_1, x_2))$, tracing backwards the path followed by the light rays (IRS method).

Once we have this, in order to obtain the value of the image in that point we make:
$I(x_1, x_2) = F(y_1(x_1, x_2), y_2(x_1, x_2))$, where $F(y_1, y_2)$ is the matrix which represents our source. In summary, we follow this procedure because the mapping $y \leftarrow x$ is single-valued whereas the $y \rightarrow x$ is multi-valued. We have to keep in mind that this correspondence is only an approximation, because the inverse image of a pixel of the lens plane would not match exactly to any pixel in the source plane.

The code has auxiliar procedures to change pixels into coordinates, $\overrightarrow{x} = (x_1, x_2)$, and later to convert coordinates into pixels, $j_1(\overrightarrow{y})$, $j_2(\overrightarrow{y})$, for the plot. The change is calculated by assigning coordinates to our pixelated matrix (n x n) at the vertices of the square $((-l, -l\,),(-l, l\,), (l, -l\,), (l, l\,))$ and setting a linear transformation to transform pixels into coordinates and viceversa. In the scheme below we can see a description of the code:

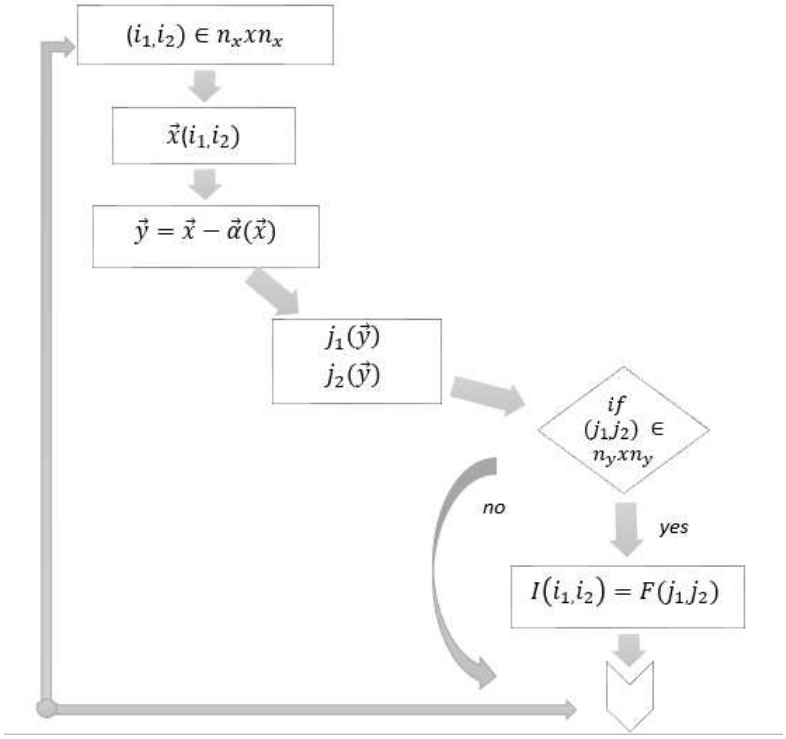

In the following pictures, we show the effect of a theoretical SIS+γ lens model on a disk-like source. We present a series of images obtained for different positions of the source along the x axis, in order to see how the images change with a moving source. The deflection angle of this type of lens is written as:

$$\alpha = \begin{pmatrix} \kappa+\gamma & 0 \\ 0 & \kappa-\gamma \end{pmatrix} x + \theta_E \frac{(x - x_d)}{|x - x_d|^2} \tag{2.1}$$

To understand this formulae, it is important to know what is the main difference between the terms convergence and shear (see eq. 1.10) and the way they affect to the final result. On the one hand, convergence is defined as a term which affects equally every possible angular orientation, that is, it would transform a certain circle in a larger or smaller one but leaving unaffected the shape of the circle. On the other hand, the shear will magnify preferably in a certain direction, that is to say, it is able to transform a circle in an ellipse with the larger axis along a privileged angle. We adopt the following values for the lens parameters: convergence (κ) equal to 0, Einstein's radius (θ_E) equal to 1 and shear (γ) equal to 0.2 (actually, it is defined as the squared root of $\gamma_1$and γ_2 which are two already fixed parameters).

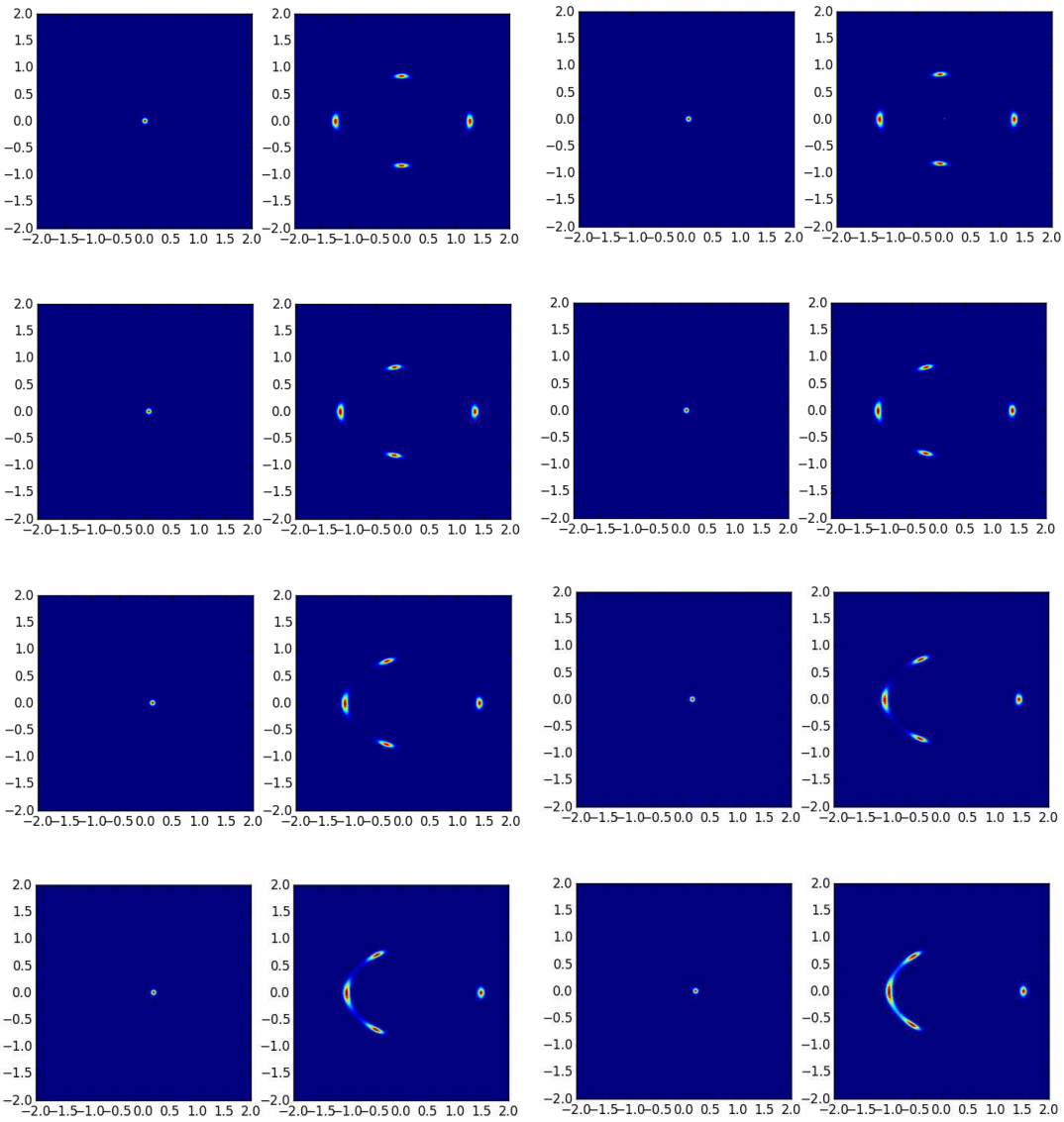

Fig 1. From the top left to the bottom right it is shown the change of the images (columns 2 and 4) originated by a SIS+γ lens when the source (columns 1 and 3) is moving towards the right. Source and lens are initially located at (0,0) with $\kappa = 0$, $\theta_E = 1$, $\gamma = 0.2$

2.2 Magnification maps

Magnification maps are an essential tool in lensing studies. Their calculation is particularly important to study quasar microlensing.

As we have seen before, the magnification measures the variation of a diferential element of area induced by gravitational lensing. In order to apply the inverse ray shooting procedure here, we can divide the lens plane in diferential elements (pixels) of area $\Delta x^1 \Delta x^2(x^1,\, x^2)$. If we consider now pixels of area $\Delta y^1 \Delta y^2(y^1,\, y^2)$ in the lens plane, the magnification in the m-pixel in the source plane will be:

$$\mu_m \quad = \quad \frac{\sum\limits_{k=1}^{N} (\Delta x^1 \Delta x^2)_k}{(\Delta y^1 \Delta y^2)_m} \tag{2.2}$$

where $(\Delta x^1 \Delta x^2)_k$ is the area of the k-pixel in the lens plane whose origin is inside the m-pixel in the source plane. This equation is valid in the approximation of tiny pixels in the lens plane where the lens inverse transformation make that each pixel of the lens plane fits within a single pixel in the source plane. If we take all the pixels of the lens plane with the same size, we can rewrite the previous equation as:

$$\mu_m \quad = \quad \frac{\sum\limits_{k=1}^{N} (\Delta x^1 \Delta x^2)_k}{(\Delta y^1 \Delta y^2)_m} = \frac{\sum\limits_{k=1}^{N} k}{\frac{(\Delta y^1 \Delta y^2)_m}{\Delta x^1 \Delta x^2}} = \frac{N}{N_0} \tag{2.3}$$

where N_0 is the ratio of areas between the pixel in the source plane and the pixel in the lens plane. The magnification will be proportional to the number of light rays that would reach a certain pixel under the action of the inverse ray shooting. To sum up, we will compute the magnification as the ratio between the number of rays that hit in a certain pixel and the number of rays that would have received this pixel in absence of lensing.

In Figure 2, it can be seen the magnification map of the same SIS+γ lens exposed in the previous section. Now the axis indicate us pixels, instead of coordinates.

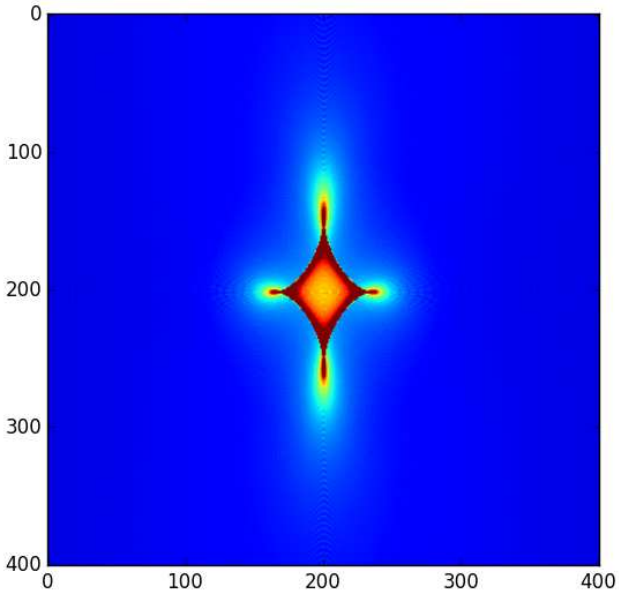

Fig 2. Magnification map corresponding to a SIS+γ lens with a background potential characterized by the same κ, γ and θ_E of the example of Figure 1.

3 Magnification of gravitational lenses proper motions

In this chapter, we use the Python based codes developed in section 2. in order to simulate the relative motions of the images of lensed quasars. In section 3.1. we introduce the concept of peculiar motion and motivate the objectives of our work. In section 3.2. we describe the effects of lensing magnification in the quasar images motion. These effects are quantified in section 3.3. and finally discussed in the context of future instrumentation in section 4.4.

3.1 Motivation and description of the phenomenon. Main objectives.

It is a well known fact that the entire Universe is expanding and galaxies should be receding from the Earth according to Hubble's law. However, the 'Hubble Flow' is alterated by the attraction between galaxies and larger structures. The universe is not composed of a smooth and homogenous matter, but of huge accumulations of matter (granulations) and vacuum between these accumulations.

Thus, all the galaxies are feeling this attraction and that's why they will have a velocity different from the expected. Then, these deviations with respect to what we call 'Hubble Flow', peculiar velocities, are really interesting to study the distribution of matter in the universe, as well as

the existence of dark matter and how it is related to these motions.

Consequently, peculiar velocities are useful to test the large-scale structure of the universe as they allow us to study the variations of the gravitational field induced by the clustering of galaxies and even greater structures. We will not go into further details of this because they are beyond the scope of this work.

Peculiar velocities are not easily measured. Let's take the example of a galaxy with a redshift z=0.3 and with a transverse peculiar velocity of 1000 km/s. The angular velocity measured by us is given by:

$$\frac{v_t}{D_{OL}} \backsimeq \frac{v_{pec}(z_l)}{1+z_l}\frac{1}{D_{OL}} \tag{3.1}$$

where z_l is the redshift of the galaxy, D_{OL} is the angular distance between the galaxy (lens) and the observer in Mpc and $v_{pec}(z_l)$ is the transverse peculiar velocity. The $(1+z_l)^{-1}$ factor transforms the time from the galaxy to the observer.

In order to determine angular distances, we used a cosmological calculator (Ned Wright's Javascript Cosmology Calculator - UCLA, *http://www.astro.ucla.edu/~wright/CosmoCalc.html*) and set the parameters of: flat universe with $\Omega_m = 0.286$ and $\Omega_n = 0.714$, redshift z=0.3 and the Hubble constant as $H_0 = 69.6$ (default parameter), and finally we got: $D_{OL} = 926.9\,Mpc$. If now, we substitude all these parameters in (3.1) and then, we convert this quantity into microarcsec per year, we will find that the source has an apparent motion of: 0.18 μas/year. This quantity is very difficult to measure; in fact, the maximum astrometric accuracy that can be reached (using Very Long Baseline Interferometry, VLBI) is about 10 μas . However, we know that gravitational lenses can magnify the space by a factor of several tens, and thanks to this property we would be able to measure relative movements between lens galaxy and imaged quasar which seemed to be impossible to see, otherwise.

Gravitational lenses magnify the space and, as a consequence of this, the velocity will be also magnified. Consequently, the first objective of the present work is to simulate the relative motion of lensed quasar images in order to study if it is possible to use them to determine peculiar velocities.

3.2 Animated motions of the lensed images in the cases of the quadruple lens systems: SDSS0924+0219, RXJ1131-1231, Q2237+0305

In this section, we are going to give a qualitative description of the movements of the lensed images for these 3 quadruple lens systems. We have selected these systems because of their high magnification. To do that, we will change the direction of our source along the x axis and after this, we will calculate the movement of the resultant images. In order to study the relative movements between pairs of images we will determine their positions and the difference between their displacements.

In the case of SDSS0924+0219 we have calculated the centroids of the images for each position of the source on the x axis. In order to do this, we developed a specific code in Python language which reads the matrix of the resulting image plane from our gravitational lensing simulation program and defines a function which finds any region with a difference in intensity with respect to the background (we select a reference parameter to establish the rate of this difference). When the code identifies those regions, it calculates the centroid of each image and then, it assigns to them a pair of coordinates (x,y). This process shoud be repeated as many times as the source changes its position. Once we obtain the position of these four images (x,y) for each displacement of the source, we can plot the proper motion of the four quasar images.

These proper motions are dominated by the proper motions of the lens galaxy (more than those of the observer or the quasar) because it is estimated that peculiar velocities on galaxies are quite larger than our motion relative to the CMB (Cosmic Microwave Background) frame.

Figure 3 shows the displacement of the images of SDSS0924+0219 when the source is moving along the x axis towards the right. In Figure 4, we show the centroids corresponding to the four images for each position of the source. We can see that the motion is qualitatively the same in both Figures but in Figure 4, it is shown the exact position of these images (x,y) and thus we can estimate the displacements between any pair of images. From both Figures we can conclude that the relative movement between components A and D would be easier to measure and images B and C could be used as references.

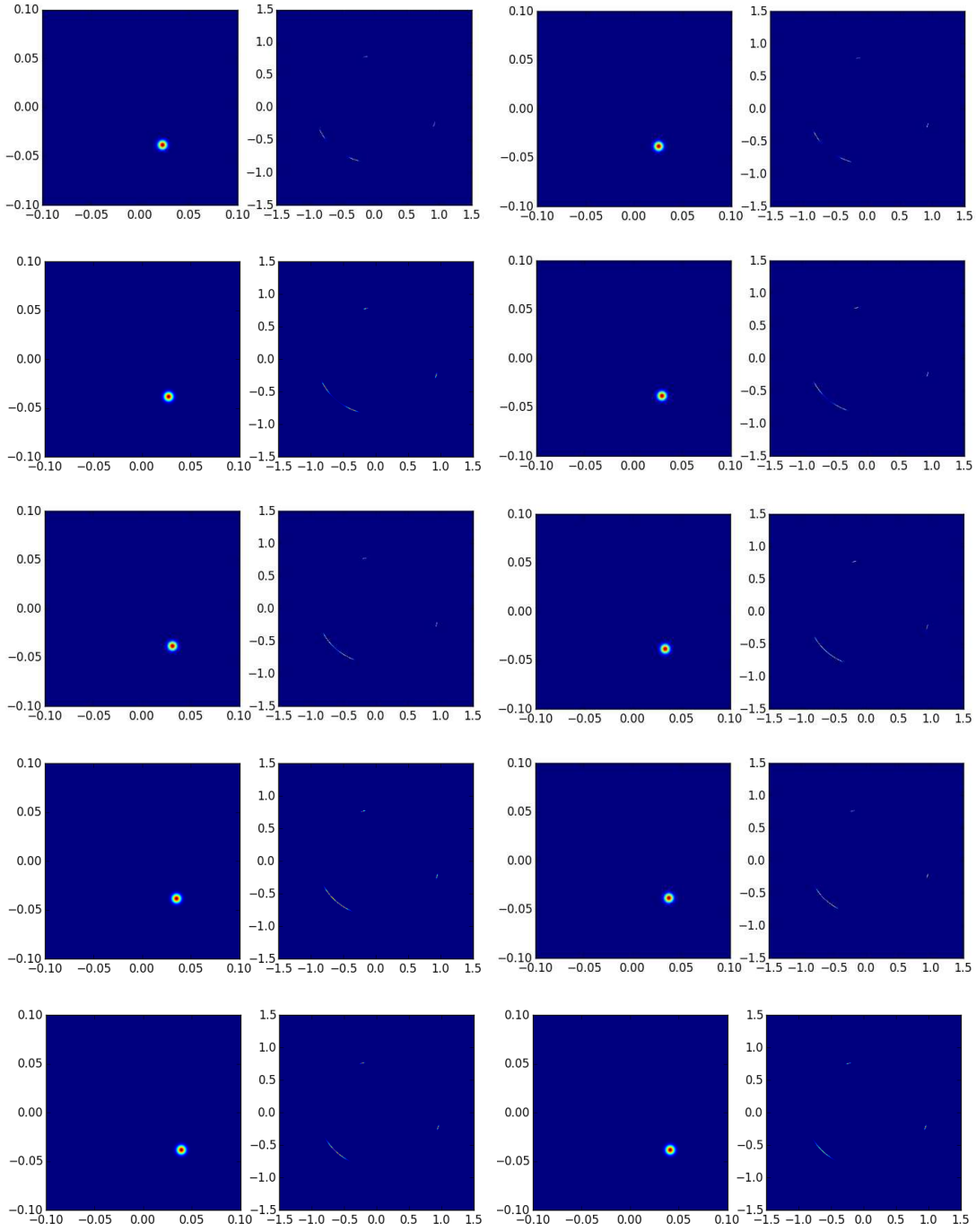

Fig 3. From the top left to the bottom right it is shown the evolution of the lens system SDSS0924+0219 when the source (columns 1 and 3) is moving to the right. The source is initially located at (0.0225829,-0.0386368) and the lens at (0,0). The parameters of the lens are: $\kappa = 0$, $\theta_E = 0.87329$, $\gamma_1 = -0.0593357$, $\gamma_2 = -0.0154813$.

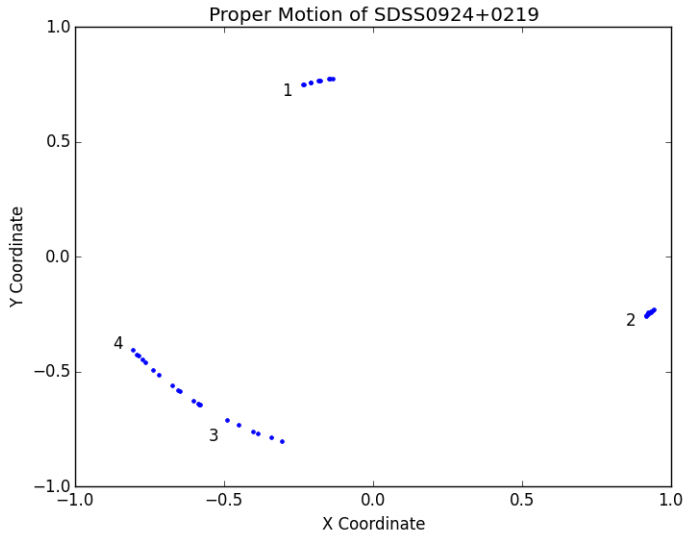

Fig 4. Proper motions of the centroids of each one of the four images. Images {1, 2, 3, 4} correspond to the real images {C, B, D, A} of the system SDSS0924+0219. Images A and D are the faster ones and it can be seen that they are approaching to each other while the source is moving to the right. Images C and B have tiny movements and its motion is comparatively negligible.

In the cases of the lens systems RXJ1131-1231 and Q2237+0305 we have not obtained the centroids (it is a time consuming calculation) but we have just done the animation when the source is now, moving to the x negative axis (to the left). The result of the simulations is presented in Figures 5 and 6.

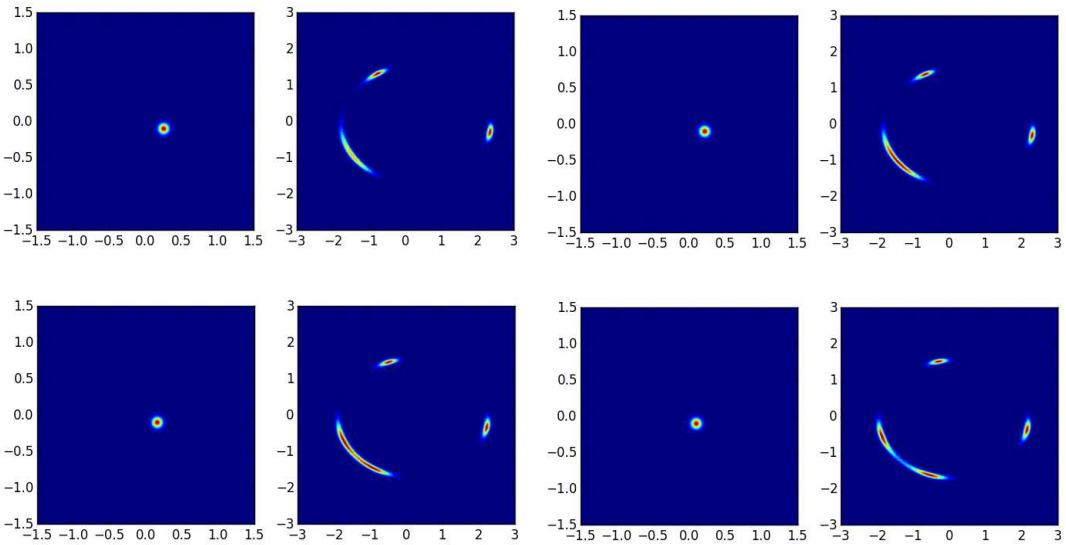

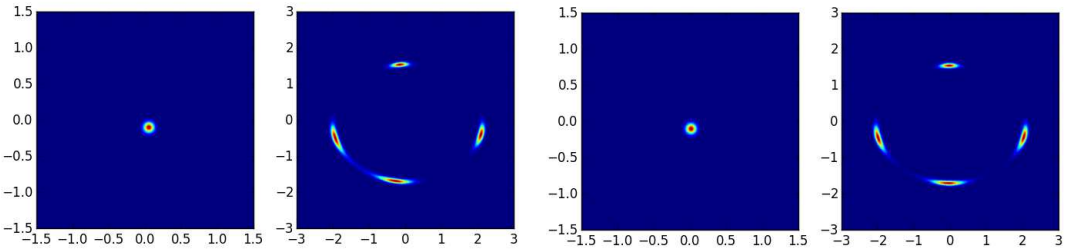

Fig 5. From the top left to the bottom right it is shown the evolution of the lens system RXJ1131-1231 when the source (columns 1 and 3) is moving to the left. The source is initially located at (0.387712,-0.102272) and the lens at (0,0). The parameters of the lens are: $\kappa = 0$, $\theta_E = 1.81752$, $\gamma_1 = -0.107849$, $\gamma_2 = 0.0511613$.

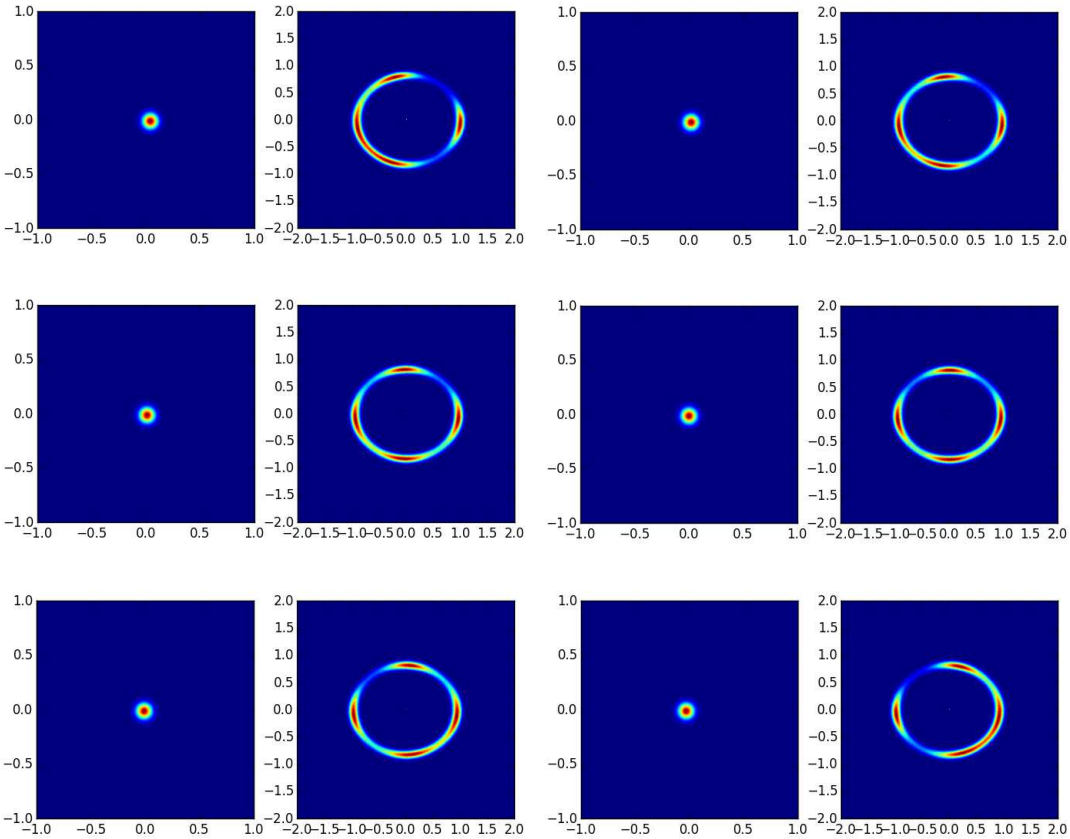

Fig 6. From the top left to the bottom right it is shown the evolution of the lens system Q2237+0305 when the source (columns 1 and 3) is moving to the left. The source is initially located at (0.043616,-0.0142296) and the lens at (0,0). The parameters of the lens are: $\kappa = 0$, $\theta_E = 0.882841$, $\gamma_1 = -0.0523543$, $\gamma_2 = -0.0527841$.

This last object is also known as The Einstein Cross. Owing to the singularly low redshift of its lens galaxy, it is a really interesting case to study peculiar velocities.

3.3 Expected apparent motions for several high magnification systems

The objective of this section is to determine quantitatively the displacements between images when the relative motion between the lens galaxy and the source takes a realistic value. We choose the lens galaxy is motionless and that the source can be moved in any radial direction, that is to say, not only over the x axis but also with a certain angle to this axis.
Instead of the inverse ray shooting method, which does not work very well with tiny distances, we are going to apply a linear approximation to the equation (1.9):

$$\overrightarrow{\Delta x} = [A]^{-1}\,\overrightarrow{\Delta y} \tag{3.2}$$

where the form of the matrix A is given by the equation (1.10)

If we calculate the inverse of this matrix, it will take the form:

$$[A]^{-1} = \frac{1}{|A|}\begin{pmatrix} 1-\kappa+\gamma_1 & -\gamma_2 \\ -\gamma_2 & 1-\kappa-\gamma_1 \end{pmatrix} \tag{3.3}$$

where $|A| = (1-\kappa)^2 - \gamma_1^2 - \gamma_2^2$

Our increments are vectors in two dimensions as the dimensions of the coordinates $(\hat{i},\, \hat{j})$. The factor $\overrightarrow{\Delta x}$ corresponds to the motion of the image in the lens plane and $\overrightarrow{\Delta y}$ is the tiny motion of the source. The factor $\overrightarrow{\Delta y}$ is given by the expression:

$$\overrightarrow{\Delta y} = (\left|\overrightarrow{\Delta y}\right| cos(\theta)\hat{i},\, \left|\overrightarrow{\Delta y}\right| sen(\theta)\hat{j}\,) \tag{3.4}$$

where the modulus of $\overrightarrow{\Delta y}$,$\left|\overrightarrow{\Delta y}\right|$, is the relative motion of the source in $\mu as/year$ for each system computed following the same procedure of the example in section 3.1 and θ is the angle of the movement of the source with respect to the x axis.

We apply a straightforward code written in Python, with a loop for time and other for orienta-

tion, to calculate the displacements between two images (of a quadruple lens system) during 10 years with steps of 1 year, and for 24 different directions of the source trajectory from 0° to 360°. Each image {A, B, C, D} will have its own set of parameters $\{\kappa,\gamma_1,\gamma_2\}$ from which we calculate the different increments, $\overrightarrow{\Delta x}$. The distance between two images will be the substraction between the increments corresponding to each of the images. For instance, in the case of images A and B we will have:

$$\overrightarrow{\Delta x_A} = (\Delta x_A^1, \Delta x_A^2) \tag{3.5}$$

$$\overrightarrow{\Delta x_B} = (\Delta x_B^1, \Delta x_B^2) \tag{3.6}$$

$$\overrightarrow{\Theta_{AB}} = \overrightarrow{\Delta x_A} - \overrightarrow{\Delta x_B} = (\Theta_{AB}^1,\, \Theta_{AB}^2) \tag{3.7}$$

And, finally, the modulus of the distance will be,

$$\left|\overrightarrow{\Theta_{AB}}\right| \;=\; \sqrt{(\Theta_{AB}^1)^2 + (\Theta_{AB}^2)^2} \equiv \left|\hat{\Theta}(t)\right| \tag{3.8}$$

The systems chosen for the calculation are the same quadruple lens systems presented in the previous section. We have plotted for each system, a graph showing the displacements between two images during 10 years and another graph, only for 1 year, to see clearly the dependence of the displacements with the angle. The angles vary from 0° to 360° with intervals of 15°.

- **SDSS0924+0219**

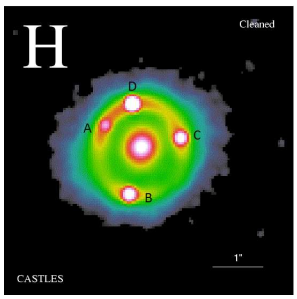

For this system we have adopted the following relevant parameters,

$z = 0.39$
$D_{OS} = 1775.1\, Mpc$
$D_{OL} = 1101.7\, Mpc$

$$|\Delta y| = 0.1428\,\mu as/year$$

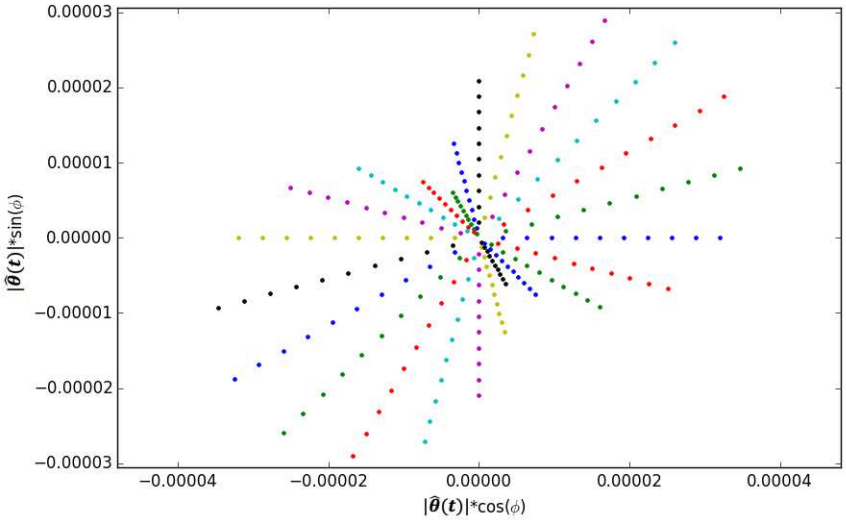

Fig 7. Graph of the displacements between images A and D of the system SDSS0924+0219 for 10 years . Each colour represents an angle and each point on the same angular position is the displacement for one of these 10 years.

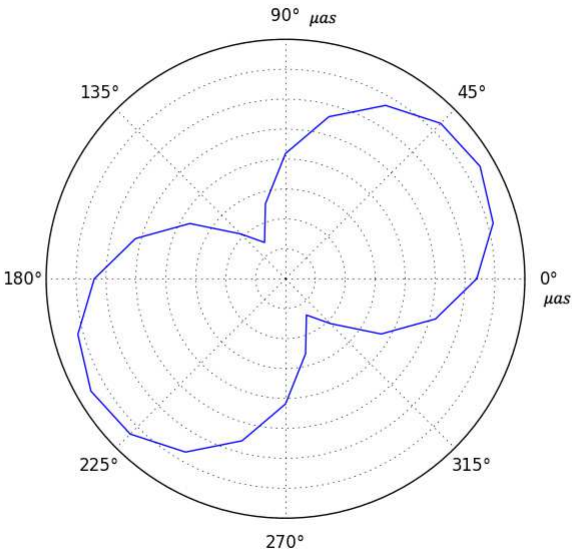

Fig. 8. Radial plot of the displacements between images A and D of the system SDSS0924+0219 for 1 year. It is represented with data from 24 angles, which starts and ends in 0°. Each radial step corresponds to 0.1 μas.

- **RXJ1131-1231**

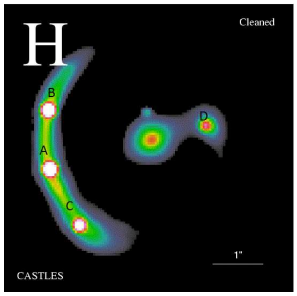

For this system we have adopted the following relevant parameters,

$z = 0.295$
$D_{OS} = 1536.3\, Mpc$
$D_{OL} = 916.1\, Mpc$
$|\Delta y| = 0.1843\, \mu as/year$

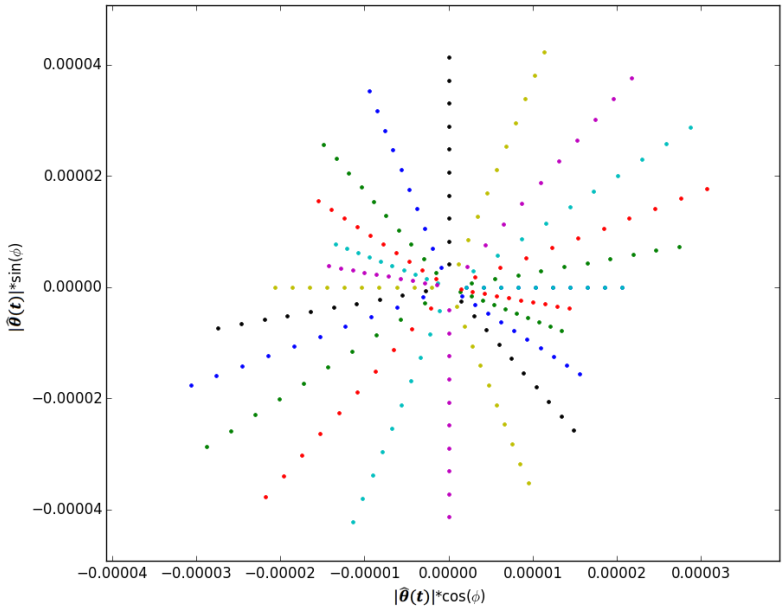

Fig 9. Graph of the displacements between images B and C of the system RXJ1131-1231 for 10 years. Each colour represents an angle and each point on the same angular position is the displacement for one of these 10 years.

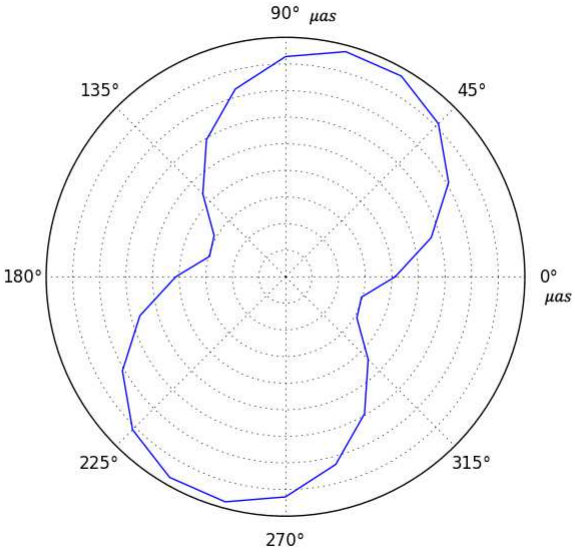

Fig 10. Radial plot of the displacements between images B and C of the system RXJ1131-1231 for 1 year. It is represented with data from 24 angles, which starts and ends in 0°. Each radial step corresponds to 0.1 μas.

- **Q2237+0305**

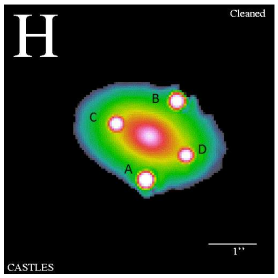

For this system we have adopted the following relevant parameters,

$z = 0.04$
$D_{OS} = 177.6\, Mpc$
$D_{OL} = 164.2\, Mpc$
$|\Delta y| = 0.7038\, \mu as/year$

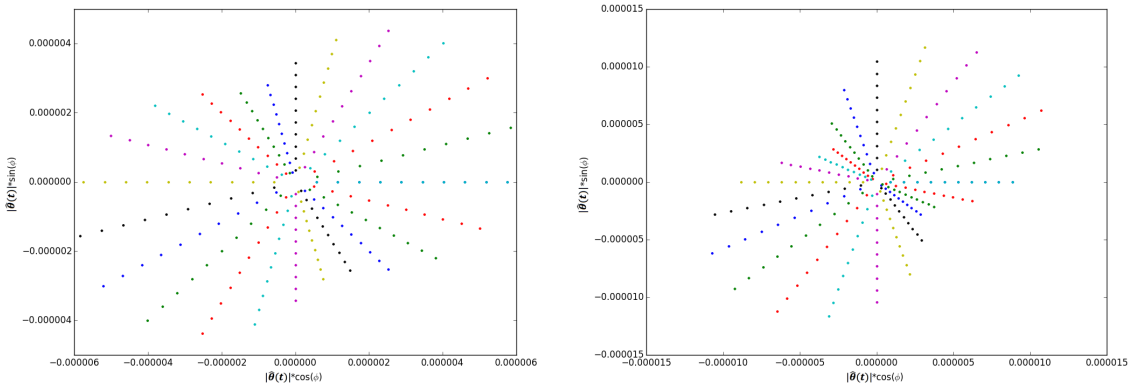

Fig 11. On the left (right) side is shown the graph of the displacements between images A and C (A and D) of the system Q2237+0305 for 10 years.

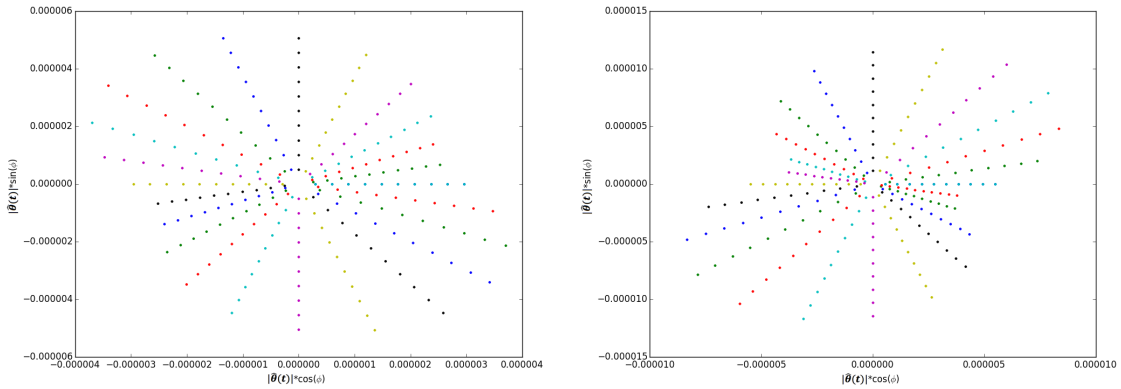

Fig 12. On the left (right) side is shown the graph of the displacements between images B and C (B and D) of the system Q2237+0305 for 10 years.

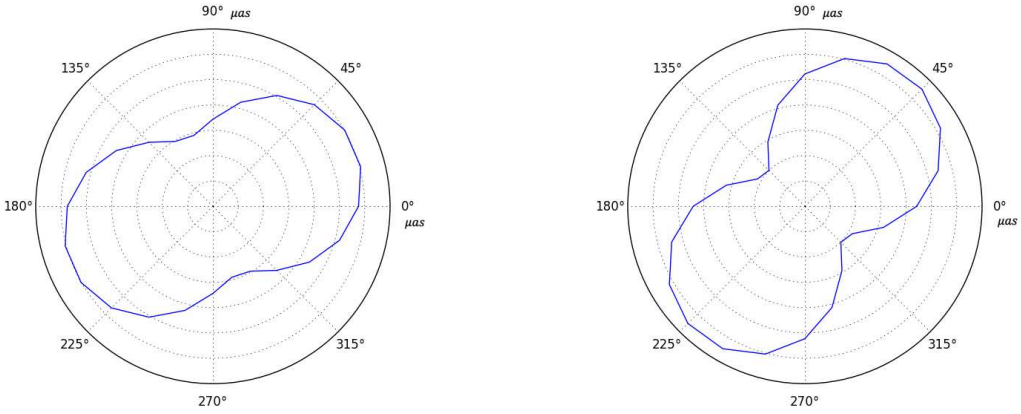

Fig 13. On the left (right) side is shown the radial plot of the displacements between images A and C (A and D) of the system Q2237+0305 for 1 year. Each radial step corresponds to 0.1 μas.

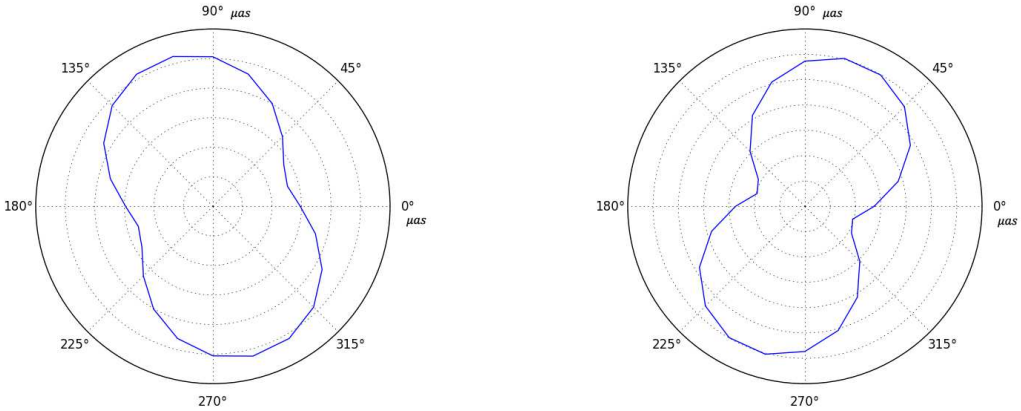

Fig 14. On the left (right) side is shown the radial plot of the displacements between images B and C (B and D) of the system Q2237+0305 for 1 year. Each radial step corresponds to 0.1 μas.

It is interesting to show the maximum displacements for 5 and 10 year corresponding to each of the considered lenses and pairs of images (see Table 1). In order to do that, we look for the angle with the maximum displacements in μas units:

Lens Systems	0924 (A-D)	1131 (B-C)	2237 (A-C)	2237 (A-D)	2237 (B-C)	2237 (B-D)
5 years (μas)	18.776	21.901	30.228	65.417	26.237	60.447
10 years (μas)	37.552	43.802	60.456	130.834	52.474	120.894

Table 1. Maximum displacements in μas between images of the quadruple lens systems chosen.

3.4 Experimental perspectives (direct or statistical detection): Gaia, HARMONI@E-ELT

Gaia is a space observatory of the European Space Agency (ESA), launched on 19^{th} December 2013, and designed for astrometry whose aim is to create an accurate 3D map or space catalog of astronomical objects and their motions. Its location is around the Sun-Earth L2 Lagragian point. Gaia is going to discover and monitor ∼2000 new gravitational lens systems with a frequency greater than once per month (i.e. one order of magnitude improvement with respect to the already known lenses).

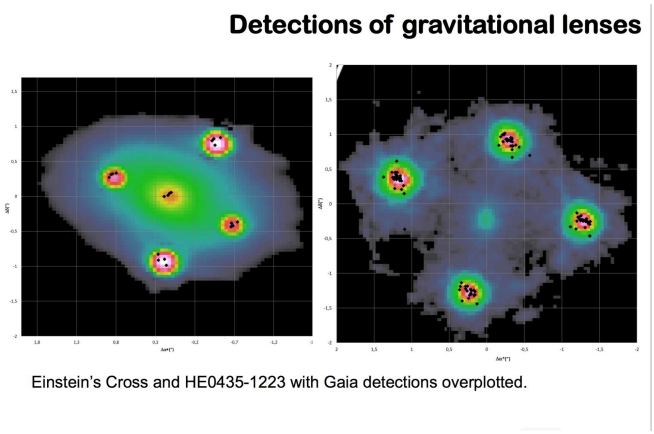

Fig 15. Sample of two systems detected by Gaia and its astrometry. In this preliminar data, the accuracy is quite far away from the nominal one. The detections correspond to the centroids (black points).

We have seen in section 3.1 and Table 1, that gravitational lenses magnify the space transforming an apparent motion of a few μas in the source to dozens of μas in the lens plane. Can Gaia measure these displacements? The accuracy of the astrometry of Gaia depends on the brightness or magnitude (V) and on the colour (V-I) of the source. Brightness can be a problem as the lensed quasar images we know are relatively weak (V>16 mag).

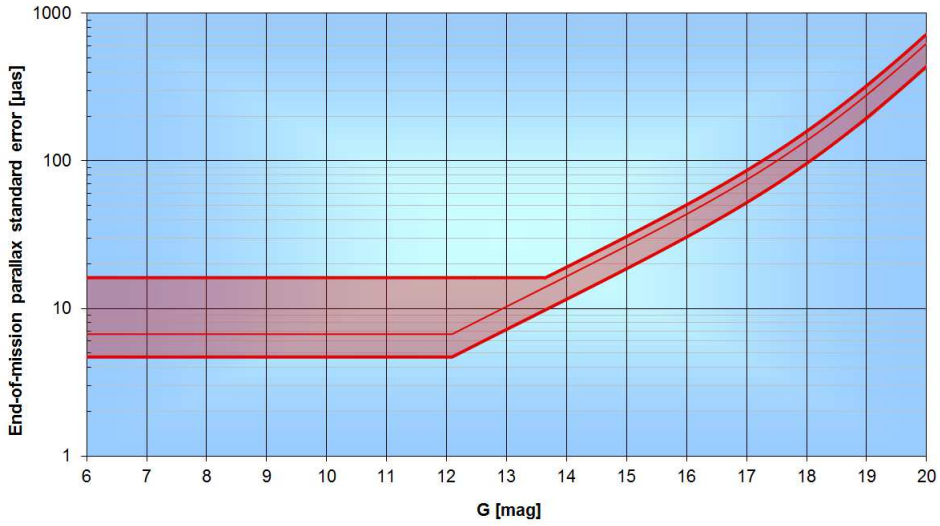

Fig 16. Proper motion standard error in μas according to the magnitude G (almost the same as V) for 5 years of astrometry in Gaia mission.

We can see in Figure 16 that for a system with a magnitude of the order of G = 16, the standard error would be between 30 and 50 μas , which is the same order of magnitude than our results. The conclusion then, is that it would not be easy to measure the displacements predicted for the present lens systems. Nevertheless, the use of Gaia can be still interesting in two different cases:

On the one hand, with the new 2000 lens systems we can expect some of them to have a higher brightness (V<16) and/or greater velocities so, in this way, we would be able to measure the displacements of individual systems.

On the other hand, we can attempt a statistical study even if the displacements are smaller than the standard error in the astrometry of Gaia. To do that, we would choose as reference a sample of background quasars which are not affected by lensing. We would measure the typical deviation in the positions along the years of monitoring of this sample and assume that they correspond to the error in the astrometry of Gaia. After that, we would also measure the displacements of our sample of lensed quasars and compare the rms (root mean square) proper motions of both samples.
The typical peculiar velocity deviation will be:

$$\sigma_{pec} = \sqrt{\sigma_{TOT}^2 - \sigma_{err}^2} \tag{3.9}$$

where σ_{err} is the typical deviation of the sample of unlensed quasars and σ_{TOT} is the typical deviation of the lensed quasar images.

We can suppose that the value of σ_{err} is the standard error of Gaia, $50\,\mu as$. Then, we can estimate σ_{TOT} from:

$$\sigma_{TOT} = \sqrt{\sigma^2_{pec(sim)} + \sigma^2_{err}} \tag{3.10}$$

where $\sigma_{pec(sim)}$ are the values calculated in the simulations of section 3.3.

Now, we want to calculate the relative error of σ_{pec}. From equation (3.9) and the standard error in the typical deviation formula, we obtain:

$$\frac{\Delta\sigma_{pec}}{\sigma_{pec}} = \left(\frac{\sigma^2_{TOT}}{\sigma^2_{pec}}\right)\left[\frac{1}{2(n-1)}\right]^{1/2} \tag{3.11}$$

where n is the number of possible images of which we can obtain measurements. The value of σ_{TOT} can be known by applying the formula (3.10).

We are going to suppose that, at least, 1 of 10 lenses discovered by Gaia (they are in total 2000) will have pair of images with a displacement of about 30 μas. Then, the number we must apply to the equation (3.11) will be $n = 200$, and in that case, we would obtain $\frac{\Delta\sigma_{pec}}{\sigma_{pec}} = 0.19\,\mu as$.

In Table 2, it is shown the maximum displacement in μas of each system for 5 years, $\sigma_{pec(sim)}$, and the result of the relative error of σ_{pec}.

Lens Systems	0924 (A-D)	1131 (B-C)	2237 (A-C)	2237 (A-D)	2237 (B-C)	2237 (B-D)
$\sigma_{pec(sim)}(\mu as)$	18.776	21.901	30.228	65.417	26.237	60.447
$\frac{\Delta\sigma_{pec}}{\sigma_{pec}}(\mu as)$	0.405	0.311	0.187	0.079	0.232	0.084

Table 2. Maximum displacements for 5 years and their relative error, everything in μas.

Even though the measurement can be statistically achieved, the best way to successfully approach this study is to extend the period of observation with Gaia. An enlarged mission will also significantly increase the number of individual astrometric measurements.

On the other hand, HARMONI@E-ELT is an instrument which consists of a visible and near-infrared integral field spectrograph that will be able to work close to the difraction limit of the telescope E-ELT (European Extremely Large Telescope) and it is expected to start operating in 2024. HARMONI will provide us an astrometry with an accuracy between 10 and 50 μas, even for V>19. It means that it will allow us to measure our lens systems more comfortably than Gaia.

4 Extreme events (caustics as peaks with very high threshold) statistics

The simulation of the light-curves of a quasar and the count of their relative maxima is the main goal of this chapter. In section 4.1. we explain how this can be used to estimate peculiar velocities. Then we compute, for the lensed system Q2237+0305, magnification maps (section 4.2.) and extract slices from these maps which simulate microlensing light curves (section 4.3.). Finally, in section 4.4., we study the number of maxima in those light curves.

4.1 Motivation and description. Objectives.

The basic idea of this chapter is that a slice of a magnification map corresponds to a light curve (how the brightness of an object can change with microlensing). The light curve changes with a fundamental frequency which comes from the spatial variations induced by microlensing. The idea to measure peculiar velocities is to compare the frequency of the temporal variability of microlensed quasar images (inferred from observed light curves) with this fundamental spatial frequency (inferred from magnification maps). Both frequencies should be related by the relative velocity between the lens, the source and the observer. Here we are going to analyze several simulated light curves in order to study their variability.

In order to achieve this purpose as simpler as possible, the most favourable option can be done by counting caustic crossings on the light curves. The crossing of a caustic by the lensed source due to its relative motion with respect to the lens (galaxy) is the most outstanding event that can be seen in microlensing light curves.

Caustics are located randomly and we asume that, even though the distances between them are not the same, in the average there are the same number of caustics per unit space. Then, caustics can be treated as randomly distributed milestones of known mean separation. When the source is travelling a certain distance, this will be proportional to the number of crossed caustics, and the typical deviation will be proportional to the square root of this number, $\propto \sqrt{N}$ (assuming a Poissonian statistics).

However, we have to take into account that caustics could be smoothed by the source size. If the source is large, it will be difficult to distinguish caustics and we could confuse them with another type of microlensing phenomenology. On the other hand, if the source is small (like an X-ray emitting region) we will be able to count caustics, so this would be the optimal choice. Unfortunately, the X ray light curves are not available for doing measurements and instead, we

need to use the more accesible wavelengths (optical) where the sources are large. Thus,we are going to use an obvious generalization: the count of all the peaks of the light curve. These peaks include caustic crossings and other microlensing phenomenology. To avoid problems with any kind of noise we are going to consider only the peaks over a certain threshold (Peaks Over a Threshold, POT).

In a few words, the aim of this chapter is to simulate light-curves from magnification maps and design a procedure to count POTs.

4.2 Magnification maps of the quadruple lens system Q2237+0305

In this section we want to describe the computation of microlensing magnification maps for the system Q2237+0305 , using a code written in Python programming language. First of all, it is needed to set a few parameters as κ, γ, α (the mass fraction of the microlenses, which is 0.999), the number of pixels (ny), the number of rays per pixel in absence of lensing effect and the half size of the magnification map in units of the Einstein radius (y_l).

The program generates the number and the positions of microlenses considering a random distribution of stars. The rays were deflected according to the lens equation. This deflection contains an inner loop over all the deflectors. With the coordinates of the deflected rays at the source plane, then we calculate the coordinates of the pixel on which each ray hits and, if it is whithin our region of interest, the program adds 1 to the value of that pixel. Finally, when the loop over rows of rays ends, we normalize the magnification map by dividing the array by the number of rays per pixel in absence of lensing.

The program generates two different maps: the first one which shows the rectangular shooting region of the light rays and the position of the stars in the background, and the second one which is the matrix representing the magnification map. We have generated magnification maps for the A and D images of the system Q2237+0305. Each of the images have different values of shear (γ) and convergence (κ) and that is why the result of applying this program is different from each other. We have to take into account that the total convergence is splitted into a part coming from a smooth distribution of matter, $\kappa_C = (1-\alpha)\kappa$, and a part coming from compact objects, $\kappa_S = \alpha\kappa$, which is able to produce microlensing.

In Figures 17 and 18, we can see the quasar microlensing magnification maps for the images A and D of the system Q2237+0305 (Einstein Cross):

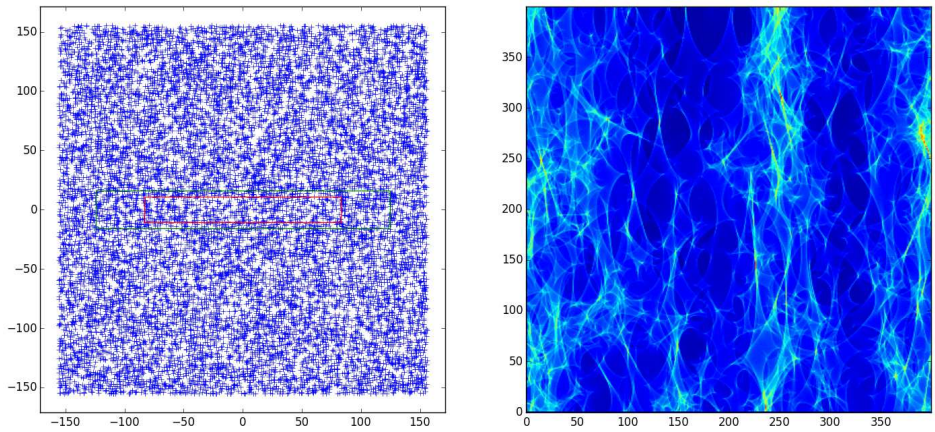

Fig 17. Magnification map for image A of Q2237+0305. The size of the map is $20\theta_E$ and it has 400x400 pixels. The parameters for the calculation are $\kappa = 0.47$, $\gamma = 0.41$. On the left, the lens plane with the position of the 14436 stars. The ray-shooting region is marked by the green square and the mapped region by the red square.

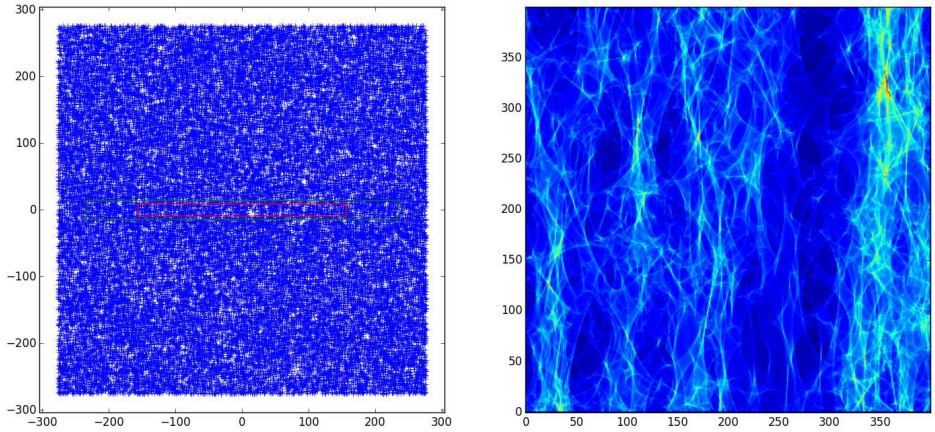

Fig 18. Magnification map for image D of Q2237+0305. The size of the map is $20\theta_E$ and it has 400x400 pixels. The parameters for the calculation are $\kappa = 0.50$, $\gamma = 0.57$. On the left, the lens plane with the position of the 48082 stars. The ray-shooting region is marked by the green square and the mapped region by the red square.

4.3 Light-curves POT counts

Once we have the quasar microlensing magnification maps for each image {A, D} of the system Q2237+0305, our program extracts an horizontal slice on these magnification maps (a simulated light curve) and searches the corresponding maxima in the light curves.

In order to qualify a maximum as POT, it is required that, in a window of side 2·dx, the maximum is greater than a given threshold; formally it is:

$$\frac{f\,[i]}{f\,[i+dx]} > threshold \tag{4.1}$$

$$\frac{f\,[i]}{f\,[i-dx]} > threshold \tag{4.2}$$

We have made some estimates of the window size with the idea that the window were broader than a typical peak but also, smaller than the separation between two consecutive peaks. We found that values in the range of $dx \sim 5-10$ pixels could be reasonable. At the end, we have considered both values in the computation.

Finally, the program gives us the x coordinates (location in pixels) of each POT found. We have done this procedure for 7 horizontal slices, since the pixels go from 0 to 400, the horizontal slices are located at 50, 100, 150, 200, 250, 300, 350. In addition to that, we have considered 6 different thresholds in order to delve deeper into the study. At the end, we have a graph for each horizontal slice (and for each image of the system) and a certain number of POTs calculated for each threshold as many times as horizontal slices we have.

In Figures 19 to 25, we show the graphs for each slice and for each image of the system {A, D} in the case of the window $dx = 10$ (as an example). We have plotted on the graphs the POTs found in the form of coloured dots, choosing for this purpose the 1.5 and the 2.4 thresholds. Our thresholds (see equations 4.1 and 4.2) were 1.1, 1.2, 1.5, 1.8, 2.1 and 2.4. Obviously, for a relative maximum of 1.5 we will find more POTs than in the case of 2.4. In Tables 3 and 4 we present the number of POTs found, the mean value of this number for each threshold and the standard deviation, everything calculated for both images.

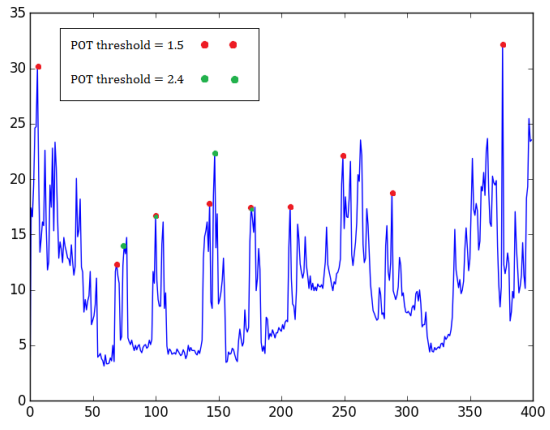

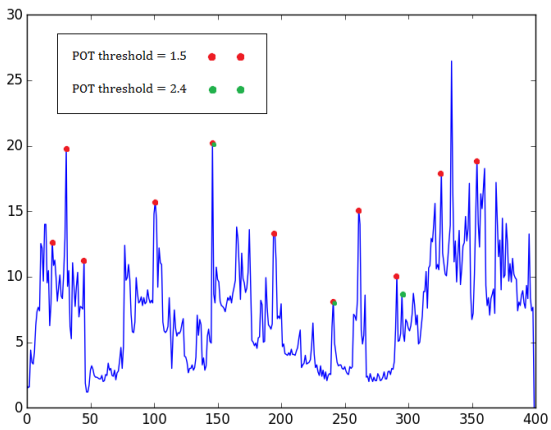

Fig 19. Light-curves for a horizontal slice located at the pixel 50 in the vertical axis of each magnification map. On the left (right) we have the light curve for the image A (D). The x axis corresponds to the pixels of the magnification maps and the y axis is the magnification.

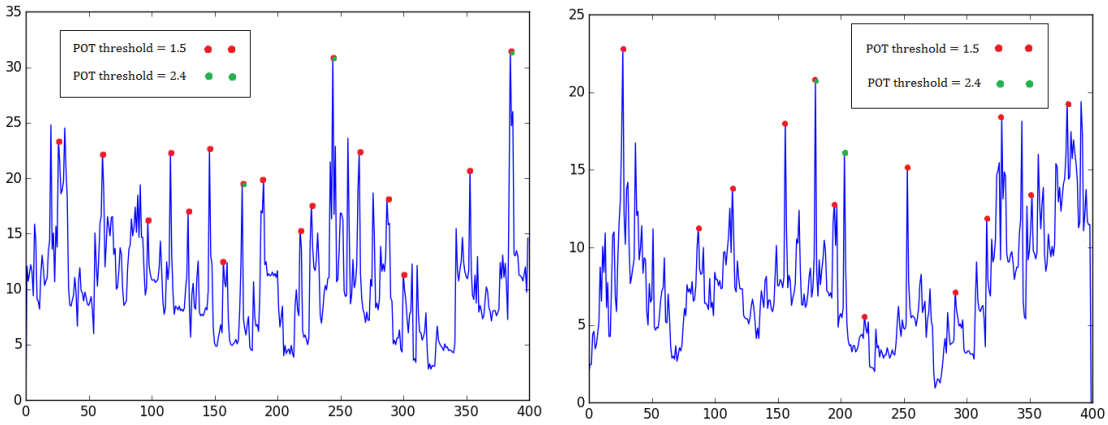

Fig 20. Light-curves for a horizontal slice located at the pixel 100 in the vertical axis of each magnification map. On the left (right) we have the light curve for the image A (D). The x axis corresponds to the pixels of the magnification maps and the y axis is the magnification.

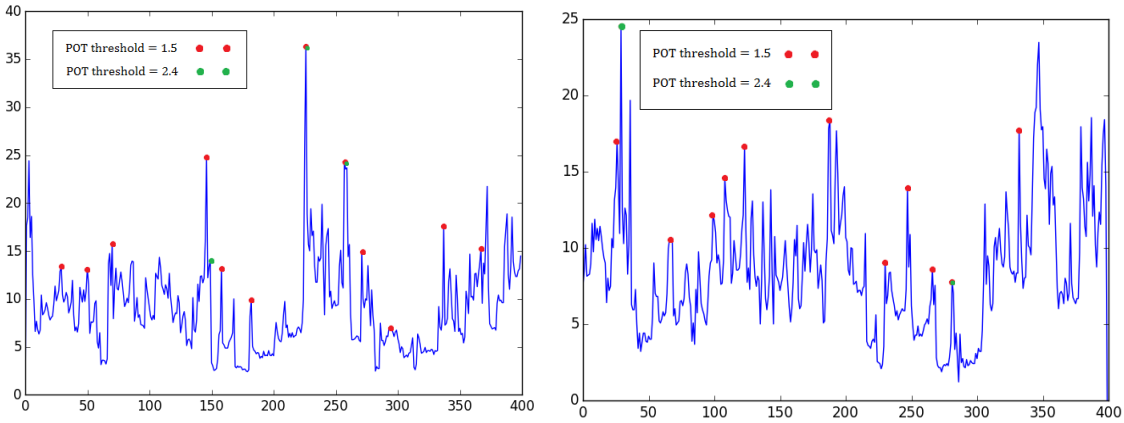

Fig 21. Light-curves for a horizontal slice located at the pixel 150 in the vertical axis of each magnification map. On the left (right) we have the light curve for the image A (D). The x axis corresponds to the pixels of the magnification maps and the y axis is the magnification.

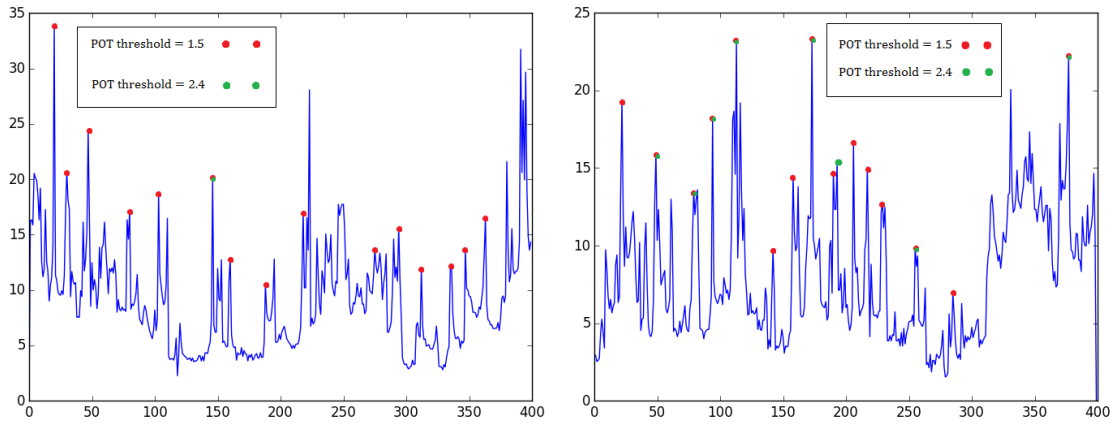

Fig 22. Light-curves for a horizontal slice located at the pixel 200 in the vertical axis of each magnification map. On the left (right) we have the light curve for the image A (D). The x axis corresponds to the pixels of the magnification maps and the y axis is the magnification.

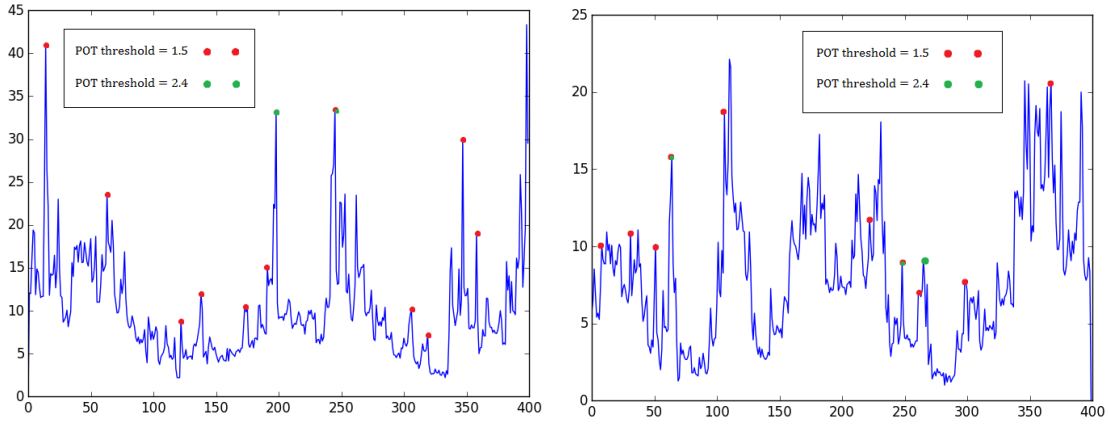

Fig 23. Light-curves for a horizontal slice located at the pixel 250 in the vertical axis of each magnification map. On the left (right) we have the light curve for the image A (D). The x axis corresponds to the pixels of the magnification maps and the y axis is the magnification.

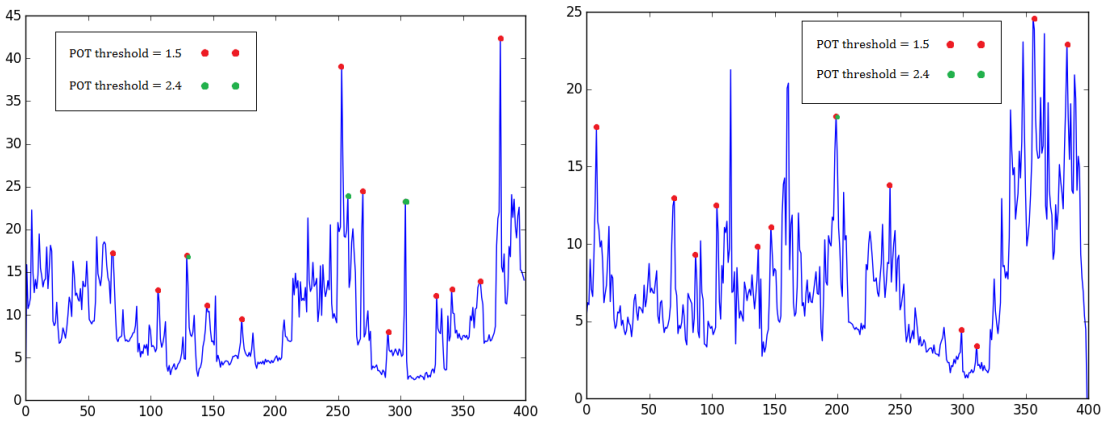

Fig 24. Light-curves for a horizontal slice located at the pixel 300 in the vertical axis of each magnification map. On the left (right) we have the light curve for the image A (D). The x axis corresponds to the pixels of the magnification maps and the y axis is the magnification.

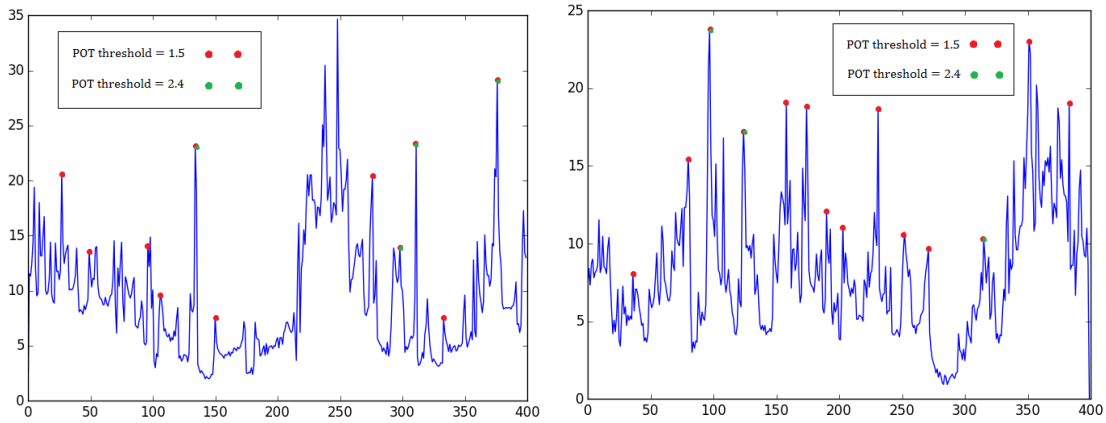

Fig 25. Light-curves for a horizontal slice located at the pixel 350 in the vertical axis of each magnification map. On the left (right) we have the light curve for the image A (D). The x axis corresponds to the pixels of the magnification maps and the y axis is the magnification.

In the Figures, we can appreciate that some of the green dots (threshold 2.4) coincide with the corresponding red dots in the same graph (threshold 1.5). This demonstrates that the program detects the POTs in a consistent way.

- **Case of the image A (dx=10, dx=5):**

Thresholds	1.1	1.2	1.5	1.8	2.1	2.4	1.1	1.2	1.5	1.8	2.1	2.4
Slice 50	20	17	9	6	4	4	27	25	13	5	2	2
Slice 100	23	21	17	13	5	3	34	29	16	10	7	4
Slice 150	19	19	12	9	4	3	32	22	9	6	4	2
Slice 200	21	20	15	9	8	1	32	31	20	15	8	1
Slice 250	19	16	11	6	3	2	36	30	18	8	4	4
Slice 300	21	20	12	8	5	3	30	26	16	7	5	3
Slice 350	24	22	11	7	4	4	30	25	13	8	6	6
$< N >$	21	19.29	12.43	8.29	4.71	2.86	31.57	26.86	15	8.43	5.14	3.14
σ_N	1.91	2.14	2.70	2.43	1.60	1.07	2.94	3.24	3.65	3.31	2.03	1.68
$\sqrt{< N >}$	4.58	4.39	3.53	2.88	2.17	1.69	5.62	5.18	3.87	2.90	2.27	1.77

Table 3. Number of POT for the image A of the system Q2237+0305, for each of the slices and for both windows ($dx = 10$, $dx = 5$). It is also shown the mean value, the standard deviation and the square root of the mean number.

- **Case of the image D (dx=10, dx=5):**

Thresholds	1.1	1.2	1.5	1.8	2.1	2.4	1.1	1.2	1.5	1.8	2.1	2.4
Slice 50	21	18	11	8	6	3	31	28	14	7	4	1
Slice 100	23	19	13	8	4	2	35	30	16	11	6	4
Slice 150	24	22	11	6	4	2	35	29	20	8	4	2
Slice 200	20	18	15	11	10	8	33	29	20	15	9	4
Slice 250	19	18	10	7	3	3	32	27	11	5	3	2
Slice 300	20	19	12	7	3	1	34	29	17	10	2	2
Slice 350	19	16	14	12	6	3	32	27	14	6	2	1
$< N >$	20.86	18.57	12.29	8.43	5.14	3.14	33.14	28.43	16	8.86	4.29	2.29
σ_N	1.95	1.81	1.80	2.22	2.48	2.27	1.57	1.13	3.32	3.44	2.50	1.25
$\sqrt{< N >}$	4.57	4.31	3.51	2.90	2.27	1.77	5.76	5.33	4	2.98	2.07	1.51

Table 4. Number of POT for the image D of the system Q2237+0305, for each of the slices and for both windows ($dx = 10$, $dx = 5$). It is also shown the mean value, the standard deviation and the square root of the mean number.

An interesting result is that the estimated error, σ_N, is similar or below the Poissonian one, $\sqrt{< N >}$. To end with this section, we compare the mean value of the number of POTs found with respect to the thresholds we selected (see Figures 26 and 27). It can be appreciated that the number of POTs decrease monotonically with the threshold. We can also see that the fits to a second order polynomial give similar values for the coefficients of images A and D.

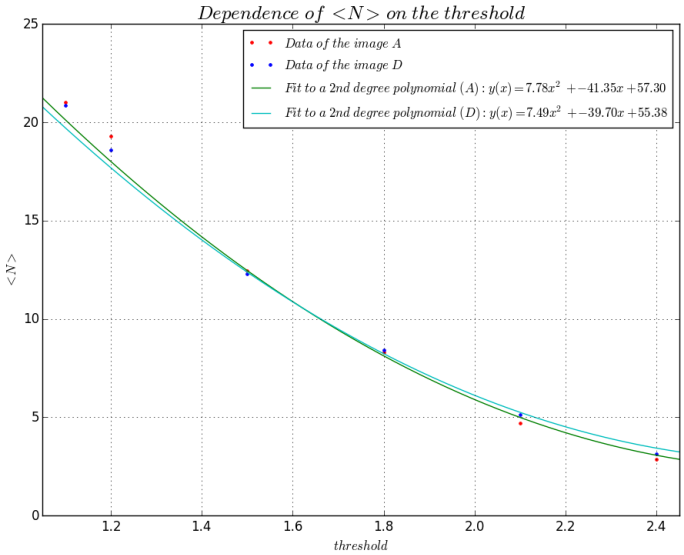

Fig 26. Relationship between the threshold and the mean number of POTs for a window of dx=10. The values for the images A and D of the system Q2237+0305 have been fitted to a second order polynomial.

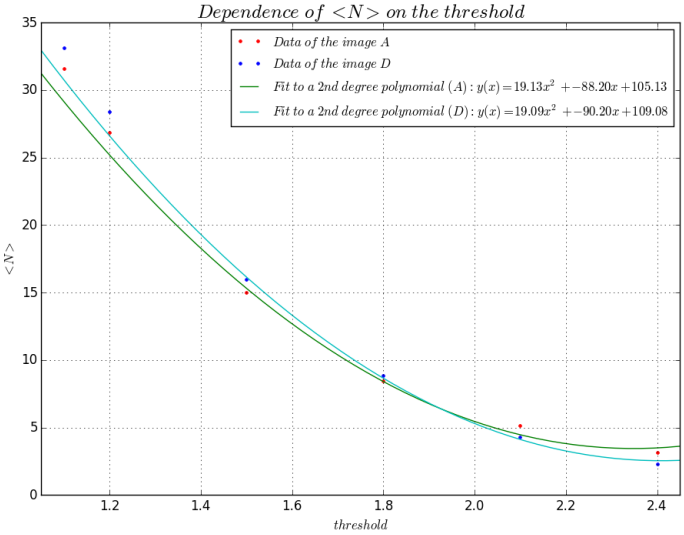

Fig 27. Relationship between the threshold and the mean number of POTs for a window of dx=5. The values for the images A and D of the system Q2237+0305 have been fitted to a second order polynomial.

5 Conclusions and future perspectives

In the first part of this work, we have developed several Python based codes to simulate the proper motions of multiple imaged quasars in order to study the possibility of measuring the peculiar velocities of lensed galaxies. The main conclusions are the following:

- The displacements we have obtained, depend on the orientation of the source motion and also on the magnification of the image.
- For a velocity of the order of 1000 km/s, which is the one we are considering in our examples, apparent displacements of tens of μas can be expected in several years of monitoring.
- Some favourable cases of high magnification events may be measured with Gaia. But many of these systems could be studied with HARMONI@E-ELT and Theia. This last project, Theia, is an instrument whose goal is to observe the Universe in motion with an unprecedented astrometric precision. It is thought to be launched around the year 2030.

In the second part of this work, we have explored the possibility of using the count of maxima in light-curves for high magnification systems in order to try to relate this to the lens galaxy peculiar velocity. For this purpose, we have written a code which allows us to count POTs. We have applied this code to the system Q2237+0305 (Einstein Cross), and the main conclusions are:

- We found that the error in the mean number of POT, obtained from the simulations, is comparable or smaller than the Poissonian value.
- We find a clear anti-covariance of the number of POT with the threshold; it can be well fitted with a second order polynomial.

In the near future it will be important to analyze the first release of the data of Gaia this autumn to be able to explore the astrometric precision and to study the real possibilities of measuring the lensed quasar proper motions. In this moment, there are less than 200 known lenses. After the Gaia release, around 2000 lenses will be known and some of them may have large magnification in brightness and velocity.

On the other hand, in a more distant future it would be interesting to simulate the observations with HARMONI@E-ELT and Theia, in order to analyze the limits of the astrometry with these instruments.

Acknowledgments

I want to specially thank my tutor who has been guiding me throughout this work, Evencio Mediavilla, and also, I would like to thank Jorge Jiménez-Vicente, for teaching me the methodology I had to follow to be able to do the simulations. Finally, I want to mention my classmate, Roberto Díaz Pérez, for his help in the computer matter and his patience when I asked him about the procedure of the codes.

References

[1] Schneider, P., Ehlers, J., Falco, E.E. (1992). *Gravitational Lenses* (Astronomy and Astrophysics Library, 1st Study Edition). Germany: Springer-Verlag Berlin Heidelberg.

[2] Mediavilla, E., Muñoz, J.A., Garzón, F., Mahoney, T.J. (2012, XXIV Canary Islands Winter School of Astrophysics). *Astrophysical Applications of Gravitational Lensing.* Jiménez-Vicente, J. (dir.). Tutorial on inverse ray shooting, University of Granada (Spain).

[3] Kochanek, C.S., Kolatt, T.S., Bartelmann, M. (1996). *Proper motions of VLBI lenses, inertial frames, and the evolution of peculiar velocities.* The Astrophysical Journal (473), 610-619.

[4] Morgan, C.W., Kochanek, C.S., Morgan, N.D., Falco, E.E. (2006). *Microlensing of the lensed quasar SDSS 0924+0219.* The Astrophysical Journal (647), 874-885.

[5] Anglada-Escudé, G., Brandeker, A., Léger, A., Sozzetti, A. (2015). *Theia - Observing the Universe in Motion*: Letter of Intent - ESA call for M4 mission - Cosmic Vision 2015-2025.

[6] Mediavilla, E. (2016). *Peculiar Transverse Velocities of Galaxies from Quasar Microlensing. Pilot Study at z ~ 0.5.* Tenerife, Spain: Canary Islands Institute of Astrophysics (IAC).

[7] Mediavilla, E. (2010). *Gravitational Lensing teaching in the Master of Astrophysics of the ULL.* Teaching Project, University of La Laguna.

[8] Wright, E.L. (2006, PASP, 118, 1711). *Ned Wright's Javascript Cosmology Calculator.* Retrieved from: http://www.astro.ucla.edu/~wright/CosmoCalc.html

[9] Kochanek, C.S., Falco, E.E., Impey, C., Lehar, J., McLeod, B., Rix, H.-W. (n.d.). *CASTLES Survey of gravitational lenses.* Retrieved from: https://www.cfa.harvard.edu/castles/

[10] Sauer, T. (Einstein Online Vol. 04, 2010). *A brief history of gravitational lensing.* Retrieved from: http://www.einstein-online.info/spotlights/grav_lensing_history#section-4